Volume 13 | Number 43 | 21 November 2015 | Pages 10581–10764

# Organic & Biomolecular Chemistry

www.rsc.org/obc

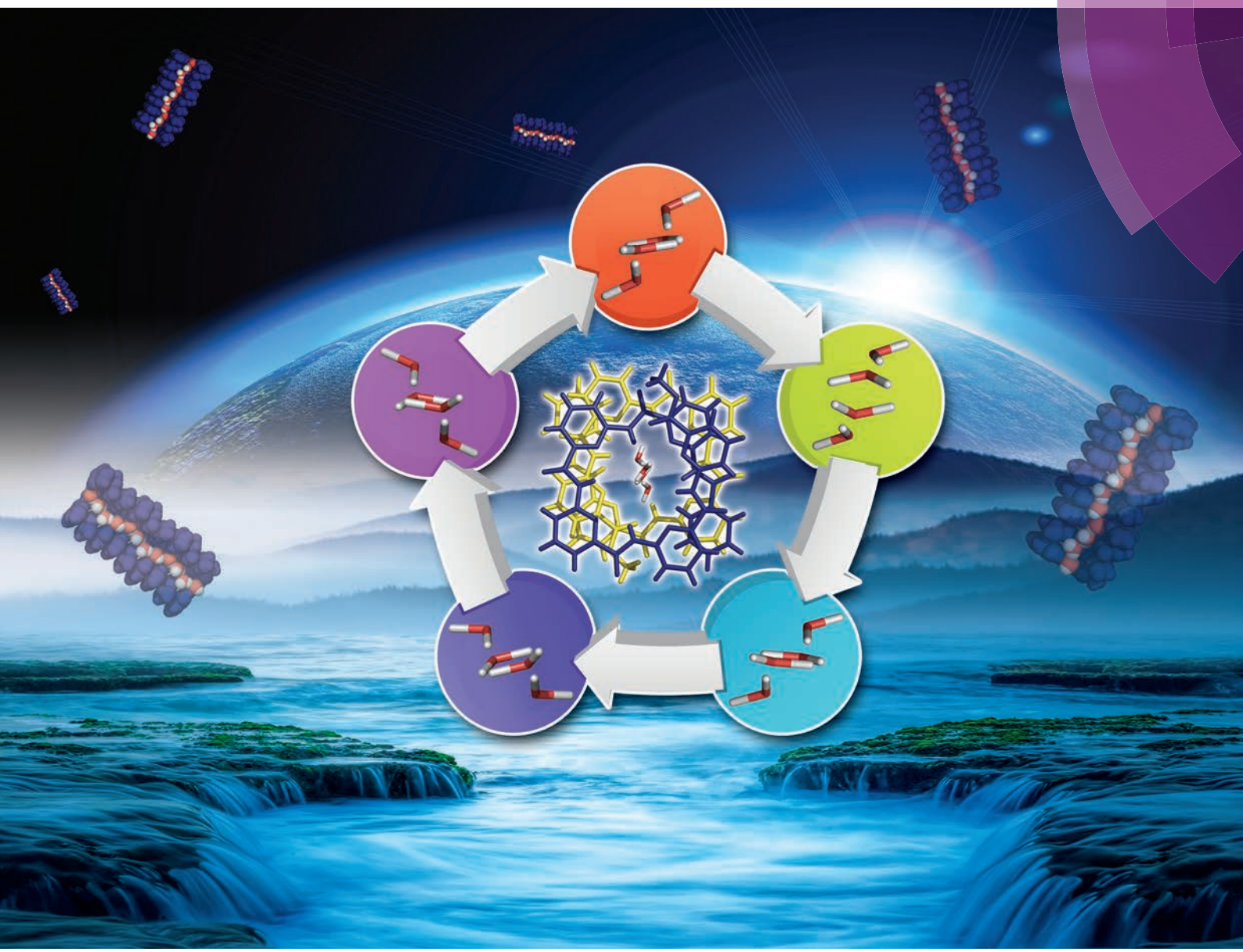

ISSN 1477-0520

ROYAL SOCIETY OF CHEMISTRY

PAPER

Yu-Jing Lu, Yanping Huo, Huaqiang Zeng *et al.*

The Dynamics, energetics and selectivity of water chain-containing aquapores created by the self-assembly of aquafoldamer molecules

Organic & Biomolecular Chemistry

PAPER

Cite this: *Org. Biomol. Chem.*, 2015, **13**, 10613

# The Dynamics, energetics and selectivity of water chain-containing aquapores created by the self-assembly of aquafoldamer molecules†

Wenliang Ma,[a] Chunquan Wang,[a] Juntong Li,[a] Kun Zhang,[a,b] Yu-Jing Lu,*[a] Yanping Huo*[a] and Huaqiang Zeng*[c]

Received 18th August 2015,
Accepted 10th September 2015

DOI: 10.1039/c5ob01732g

www.rsc.org/obc

Through a series of crystallographic snapshots of water chain-containing aquapores formed from numerous one-dimensionally aligned aquafoldamer molecules **2**, we demonstrated here (1) a preferential recognition of the water molecules over methanol molecules by the assembled cavity-containing aquapores with a selectivity factor of at least 17.7, (2) the dynamic nature of the water chains and the aquapores in response to varying external stimuli that exert the most influential impact on the aromatic π–π stacking in the aquapores and (3) the aquapores undergo a significant rearrangement in order to accommodate water, rather than methanol, molecules.

## Introduction

Inspired by aquaporins' ability to trap one-dimensionally arrayed H-bonded water chains in their narrow channels and to selectively transport water molecules,[1] we have been interested in using a supramolecular approach to mimic aquaporins in both structure and function with an ultimate aim to realize synthetic water channels for rapid and selective transport of water molecules for water purification. Such investigations are also in line with the recently emerged efforts,[2] focusing on creation of organic molecule-based hydrophilic[3] or hydrophobic[4] pores that are capable of hosting H-bonded 1D water chains and transporting water molecules[3f,5] and protons[3f,5a,6] across the bilayer membrane.

Our molecular strategy toward water recognition and transport builds upon our lasting interest in designing functional foldamer molecules[7] that are derived from methoxy,[8a–c] pyridone[8d,e] and fluorobenzene[8f,g] building blocks. These folding molecules not only are able to adopt stable, compact conformations, but also perform many interesting functions including selective recognition of both ionic[8e,9a,b] and neutral[9c,d] species, solvent gelation,[8g] reaction sieving[9e,f] and catalysis.[9g] By integrating computational modeling and crystallographic scrutiny, we recently envisioned and demonstrated the ability of intramolecular H-bonding forces to guide the folding of pyridine-based foldamer molecules such as pentamers **1** and **2** (Fig. 1) into a crescent or helically folded structure to enclose a cavity of ~2.8 Å in diameter defined by the interior amide protons.[10a] This small cavity rich in H-bond donors and acceptors matches well with the molecular dimensionality of water molecules measuring ~2.8 Å in diameter. Accordingly, short oligomers such as a trimer with a roughly planar geometry can bind one water molecule in their 2D planar cavity, while helically folded longer oligomers allow a water dimer to comfortably stay in their 3D-shaped helical cavity.[10b,c] The terms "aquafoldamer" and "aquapore" were then coined by us to describe these water-binding foldamer molecules and the pores contained within them.

Our recent continued exploration revealed that, by incorporating two electrostatically complementary functional groups into the two helical ends of helically folded aquapentamer **1**, the resultant helices possessing "sticky" ends (*e.g.*, the ester and Cbz ends) could efficiently pile up *via* aromatic π–π stacking forces to produce one-dimensionally aligned helical stacks. This 1D packing further results in a hollow tubular cavity for inclusion of guest molecules such as methanol[11a] and dichloromethane.[11b] Through further subtle structural variations, a more rigid pyridine-based pentamer **2** was eventually discovered to produce similar 1D stacks containing well-aligned H-bonded 1D water chains in the formed narrow aquapores of ~2.8 Å in diameter. Functionally, these 1D water chains selectively transport water molecules across the bilayer membranes of large unilamellar vesicles of ~250 nm in diameter.[11c]

[a]*Faculty of Chemical Engineering and Light Industry, Guangdong University of Technology, Guangdong, 510006, China. E-mail: yphuo@gdut.edu.cn*
[b]*School of Chemical and Environmental Engineering, Wuyi University, 99 Yingbin Road, Jiangmen, Guangdong, 529020, China*
[c]*Institute of Bioengineering and Nanotechnology, 31 Biopolis Way, The Nanos, Singapore 138669. E-mail: hqzeng@ibn.a-star.edu.sg; Tel: (+) 65-6824-7115*
†CCDC 1419114–1419118. For crystallographic data in CIF or other electronic format see DOI: 10.1039/c5ob01732g

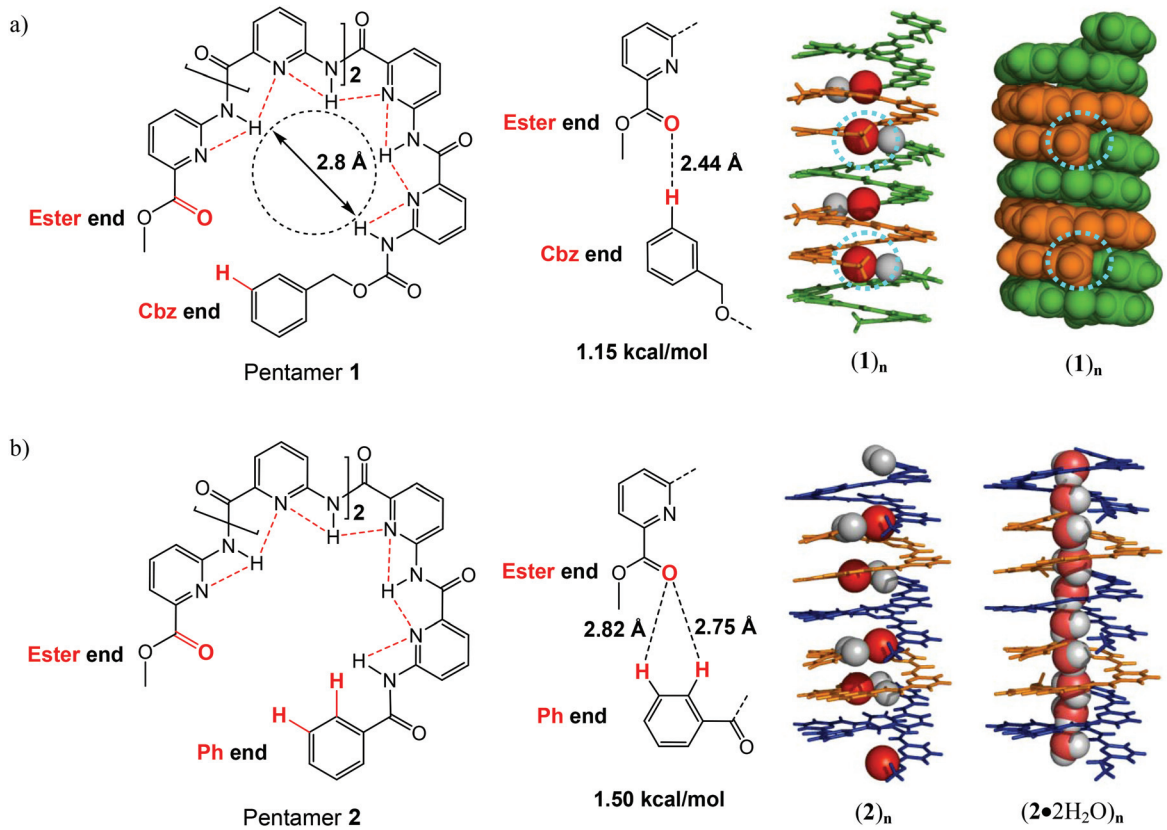


**Fig. 1** (a) and (b) illustrate the structures of pentamers **1** and **2**, respectively, which contain an interior cavity of ~2.8 Å in diameter defined by the interior amide protons, two "sticky" end groups (ester and Cbz or Ph groups) that are complementary to each other by virtue of a partially charged O-atom (H-bond acceptor) and an aromatic proton (H-bond donor) able to form weak intermolecular H-bonds of 2.44 Å, 2.75 Å and 2.82 Å with bond strengths of 1.15 and 1.50 kcal $mol^{-1}$ computationally determined at the B3LYP/6-311G(2d,p) level, 1D chiral packing involving numerous molecules of **1** or **2** *via* complementary "sticky" end groups and aromatic $\pi-\pi$ stacking forces. From the CPK model of $(\mathbf{1})_n$ shown in (a), the 1D chiral stack appears to be built from a single chiral polymeric backbone, rather than from a copious amount of short oligomers. Also shown in (b) is the well-aligned 1D water chain trapped inside the 1D chiral stack of $(\mathbf{2})_n$.

In the current work, we aim to provide additional insights into the functional hollow ensembles formed by **2** (*e.g.*, the trapped water chains and self-assembled water-binding aquapores) in terms of dynamics, energetics, and selectivity by comparing crystallographic snapshots of the system in response to varying external stimuli and by computational calculations either at the B3LYP/6-311+G(2d,p) level or using the Dreiding force field.[12a]

## Results and discussion

Our early studies show that (1) slow diffusion of methanol into **1**-containing dichloromethane ($CH_2Cl_2$) solution gives rise to crystals of **1**·MeOH containing regularly arrayed chains of methanol molecules in the hollow tubular cavity of $(\mathbf{1})_n$ [11a] and (2) slow diffusion of acetone or ethyl acetate into **1**-containing $CH_2Cl_2$ produces crystals with $CH_2Cl_2$ molecules residing in the hollow cavity.[11b] Very surprisingly, even after re-growing or soaking the crystals of **1** in water-containing solvents, all the structural determinations of crystals reveal that only 24–40% of the MeOH molecules inside the interior of $(\mathbf{1})_n$ were replaced by water molecules, suggesting that the recognition of $H_2O$ molecules is preferred over $CH_2Cl_2$ molecules by the hollow cavity in $(\mathbf{1})_n$. A partial replacement of 24–40% of the MeOH molecules by $H_2O$ is also in sharp contrast to the fact that other pentamers, differing from **1** by the two end groups, can readily accommodate two water molecules in their cavity even when the crystals were grown from anhydrous $CH_2Cl_2$.[10b,c] These data suggest that the recognition of MeOH molecules by the hollow cavity in $(\mathbf{1})_n$ takes place in a selective manner with its binding affinity toward small guest molecules decreasing in the order of MeOH > $H_2O$ > $CH_2Cl_2$ and that the hollow cavity in $(\mathbf{1})_n$ does not recognize other larger guests including acetone and ethyl acetate.

More surprisingly, we recently found that a small subtle structural modification, which involves a replacement of the more flexible Cbz group in **1** with a rigid phenyl ring as in **2**, renders molecules of **2** with the ability not only to form the desired 1D helical stacks mediated *via* two H-bonds between the two "sticky" ends but also to host H-bonded 1D water chains (see $(\mathbf{2}{\cdot}2H_2O)_n$ in Fig. 1b).[11c] Similar to **1**, the 1D helical

 

stacks made of **2** appear to be made up of a single polymeric helical backbone rather than numerous short oligomeric helices, creating aquapores with a narrow cavity of ~2.8 Å in diameter for transporting water molecules across the lipid bilayer membranes.[11c]

These recently reported water-containing crystals of **2**·2$H_2O$ were grown *via* slow evaporation of **2**-containing anhydrous $CH_2Cl_2$ at room temperature for weeks. Since commercially available anhydrous $CH_2Cl_2$ typically contains no more than 0.001% water by weight, a molar ratio of $CH_2Cl_2$ over water molecules under the crystal growth conditions can be calculated to be 5304 on the basis of their respective molecular weights of 84.93 and 18.02 g $mol^{-1}$. This points to an exceptional selectivity factor of at least 5304 in recognizing water over $CH_2Cl_2$ molecules by the aquapore contained in $(\mathbf{2})_n$.

A few of the other intriguing questions we attempt to answer in this work concern the ability of the aquapore contained in the helical stack of $(\mathbf{2})_n$ to accommodate other non-water molecules and the binding selectivity among the molecules that can be recognized by the aquapore. In this regard, a slow diffusion of an equal volume (1 ml) of either acetone, ethyl acetate, acetone or methanol into **1**-containing $CH_2Cl_2$ solution produces either no or crystals of **2**·MeOH containing regularly arrayed chains of MeOH molecules in the hollow tubular cavity of $(\mathbf{2})_n$, suggesting that the recognition of either water or MeOH molecules by the aquapore in $(\mathbf{2})_n$ proceeds in a selective manner.

Structural analysis of **2**·MeOH reveals the expected existence of a strong intramolecular H-bonding network that restricts the conformational freedom of the amide bonds in **2** and induces its aromatic backbone to curve in one direction, and eventually into a helical conformation (Fig. 2a). Similarly, the end ester and phenyl groups (Fig. 1b) designed to be complementary and "sticky" do stick to each other to form one moderate H-bond of 2.405 Å and one very weak H-bond of 3.018 Å between the ester carbonyl O-atom and phenyl aromatic protons. These numerous weak but attractive H-bonding forces work together with aromatic π–π stacking forces to enable numerous short helices to efficiently pack on top of each other to produce an enclosed hollow cavity of about 2.75 Å in diameter, which allows small MeOH molecules to sit inside the cavity interior *via* stabilizing strong H-bonds of 2.094 and 2.352 Å and many other weak H-bonds and van der Waals interactions between the host and guest molecules (Fig. 2b). Computationally by using the Dreiding force field[12a] for calculating aromatic π–π stacking forces and the first principles calculation at the B3LYP/6-311G(2d,p) level for H-bonds formed by "sticky" ends and MeOH stabilization by the host, it was found that efficient full overlap of helical backbones of **2** *via* aromatic π–π stacking provides the major driving force, contributing 32.04 kcal $mol^{-1}$ per molecule of **2** to the formation of 1D helical stack. This full overlap is made possible as a result of the two feeble yet indispensable intermolecular H-bonds of 1.96 kcal $mol^{-1}$ in strength arising from the two "sticky" ends. Every host molecule of **2** provides additional average stabilization energy of 9.11 kcal $mol^{-1}$ per MeOH molecule.

From the above analyses, it can be seen that the aquapores in $(\mathbf{2})_n$ selectively recognize water and MeOH molecules over other small molecules including $CH_2Cl_2$, acetone, ethyl acetate, acetone, *etc*. To further discern the selectivity between water and MeOH molecules, we designed a series of crystallization experiments involving growing crystals of **2**·2$H_2O$ *via* slow diffusion of a certain volume of mixed solvents containing MeOH and $H_2O$ in varying ratios into 1 mL $CH_2Cl_2$ that contains 1 mg of **2** in a tightly capped vial over 10–15 days at room temperature (Table 1). Crystallographic analyses of all the crystals grown under the conditions tested demonstrate an invariable trapping of only water molecules, not MeOH molecules, inside the aquapores formed by molecules of **2**. On the basis of the smallest volumetric ratio of 20 μl : 800 μl for water : MeOH that corresponds to a water : MeOH molar ratio of 1 : 17.7, a selectivity factor of 17.7 can be estimated. Further considering that the aquapores are exclusively occupied by water molecules, the actual selectivity could be much higher than 17.7 by many orders of magnitude.

Remarkably similar to the structure of **2**·2$H_2O$, all the crystal structures from $\mathbf{2_1}$·2$H_2O$ to $\mathbf{2_4}$·2$H_2O$ contain a helically folded structure of **2** that stacks on top of each other to produce the 1D hollow cavity, which subsequently trapped a

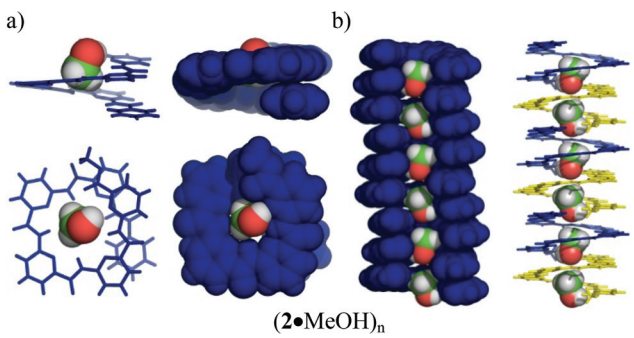


**Fig. 2** (a) Illustrates a helically folded pentameric backbone in **2** that is rigidified by an intramolecular H-bonding network and able to bind to one methanol molecule, and (b) shows 1D helical packing involving numerous molecules of **2** *via* aromatic π–π stacking forces assisted by the complementary "sticky" end groups that form H-bonds of 2.41 and 3.01 Å. From the CPK model of $(\mathbf{2}\cdot\text{MeOH})_n$ shown in (b), a discrete chain of MeOH molecules is trapped inside the hollow cavity, and no direct contacts among MeOH molecules can be seen.

**Table 1** Crystal growth conditions for **2**·2$H_2O$ and $\mathbf{2}_n$·2$H_2O$ ($n$ = 1–4) at varying ratios of MeOH/$H_2O$ (v : v) at room temperature

| | **2** | $CH_2Cl_2$ | $H_2O$ | MeOH | Crystal growth time |
|---|---|---|---|---|---|
| **2**·2$H_2O$ | 1 mg | 1 ml | 0 μl | 0 μl | 10–15 days |
| $\mathbf{2_1}$·2$H_2O$ | | | 20 μl | 10 μl | |
| $\mathbf{2_2}$·2$H_2O$ | | | | 100 μl | |
| $\mathbf{2_3}$·2$H_2O$ | | | | 200 μl | |
| $\mathbf{2_4}$·2$H_2O$ | | | | 800 μl | |

helically arrayed H-bonded 1D water chain with four water molecules per helical turn (Fig. 3a). From the top views of the water chains presented in Fig. 3b, the helically arranged water chains in $(\mathbf{2}\cdot 2H_2O)_n$, $(\mathbf{2_1}\cdot 2H_2O)_n$ and $(\mathbf{2_2}\cdot 2H_2O)_n$ might have a helical handedness different from those found in $(\mathbf{2_3}\cdot 2H_2O)_n$ and $(\mathbf{2_4}\cdot 2H_2O)_n$. A significant alteration in topology also exists for the water chains found in $(\mathbf{2}\cdot 2H_2O)_n$, $(\mathbf{2_1}\cdot 2H_2O)_n$ and $(\mathbf{2_3}\cdot 2H_2O)_n$, but those from $(\mathbf{2}\cdot 2H_2O)_n$, $(\mathbf{2_2}\cdot 2H_2O)_n$ and $(\mathbf{2_4}\cdot 2H_2O)_n$ are topologically more akin to each other if their helical handedness is not considered.

These structures additionally differ from each other in many subtle ways on how the short helices interact with each other and with the trapped water molecules as well as how the water molecules associate with each other to form the water chains. Specifically, (1) the helical pitch, which dictates the intermolecular distance between the two water molecules with an identical orientation from the 1D water chain, ranges from 10.320 Å in $(\mathbf{2_1}\cdot 2H_2O)_n$ to 10.416 Å in $(\mathbf{2}\cdot 2H_2O)_n$, (2) the average aromatic π–π stacking distance ranges from 3.440 to 3.472 Å, (3) some structural changes in the helical backbone (Fig. 4) and around the "sticky ends" are observed, (4) the two intermolecular H-bonds $H_a$ and $H_b$ (Fig. 3a) fall within 1.841–1.901 Å and 2.264–2.395 Å, respectively, and (5) the two weak intermolecular H-bonds $H_1$ and $H_2$ formed by the two "sticky" ends vary from 2.746–2.799 Å to 2.821–3.045 Å (Table 2), respectively. In terms of percent variation, intermolecular H-bonds seem to undergo the largest changes in response to the external stimulus, *e.g.*, methanol in our current study.

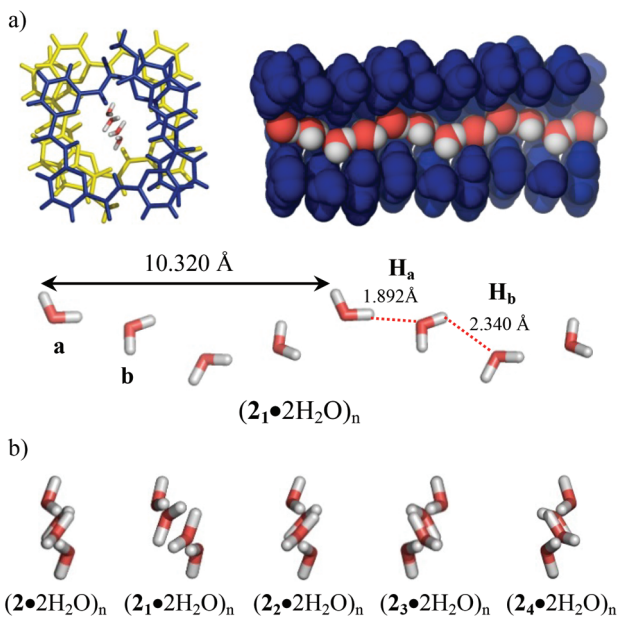


**Fig. 3** Schematic illustrations of 1D water chains taken from the crystal structure of $\mathbf{2}\cdot 2H_2O$ and $\mathbf{2}_n\cdot 2H_2O$ ($n$ = 1–4). As shown in (b), every water chain in $\mathbf{2}_n\cdot 2H_2O$ ($n$ = 1–4) also contains two types of water molecules, **a** and **b**, as well as two types of the intermolecular H-bonds, $H_a$ and $H_b$.

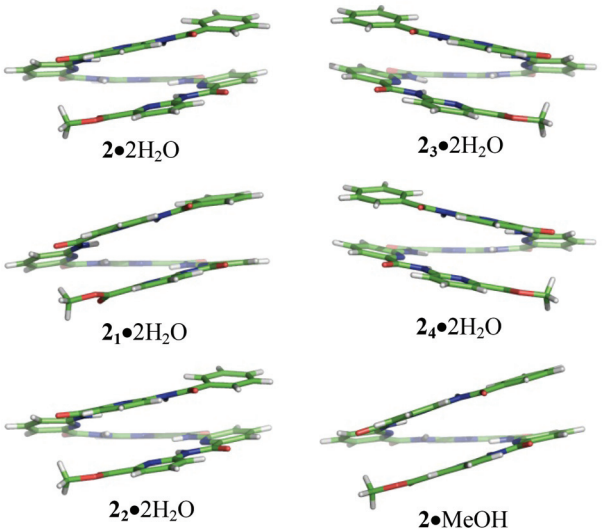


**Fig. 4** Side views of the helically folded aromatic backbone of **2** in the crystal structures of $\mathbf{2}\cdot 2H_2O$, $\mathbf{2_1}\cdot 2H_2O$, $\mathbf{2_2}\cdot 2H_2O$, $\mathbf{2_3}\cdot 2H_2O$, $\mathbf{2_4}\cdot 2H_2O$ and **2**·MeOH. Note that molecules of **2** from $\mathbf{2_3}\cdot 2H_2O$ and $\mathbf{2_4}\cdot 2H_2O$ might have a helical handedness different from others; this, however, cannot be unambiguously confirmed.

**Table 2** H-bonds formed by the two "sticky" ends from the crystal structures of $\mathbf{2}\cdot 2H_2O$, $\mathbf{2_1}\cdot 2H_2O$, $\mathbf{2_2}\cdot 2H_2O$, $\mathbf{2_3}\cdot 2H_2O$, $\mathbf{2_4}\cdot 2H_2O$ and **2**·MeOH

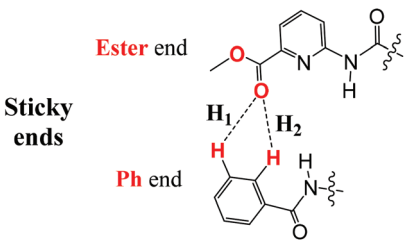


| | $\mathbf{2}\cdot 2H_2O$ | $\mathbf{2_1}\cdot 2H_2O$ | $\mathbf{2_2}\cdot 2H_2O$ | $\mathbf{2_3}\cdot 2H_2O$ | $\mathbf{2_4}\cdot 2H_2O$ | **2**·MeOH |
|---|---|---|---|---|---|---|
| $H_1$ | 2.821 Å | 3.045 Å | 2.848 Å | 2.940 Å | 2.876 Å | 2.405 Å |
| $H_2$ | 2.746 Å | 2.799 Å | 2.758 Å | 2.771 Å | 2.754 Å | 3.018 Å |

Energetically, these water chain-containing aquapores would differ in strength of the H-bonds arising from the "sticky" ends ($E_{SE}$), aromatic π–π stacking interaction ($E_\pi$), stabilization of two types of water molecules **a** and **b** (Fig. 3) with different orientations by the hosts ($E_{HG} = E_{HG_a} + E_{HG_b}$), and the two types of H-bonds $\mathbf{H_a}$ and $\mathbf{H_b}$ (Fig. 3) contained in the water chains ($E_H = E_{H_a} + E_{H_b}$). Therefore, single point energy calculations on the corresponding structural motifs directly taken out from their respective crystal structures were carried out by using the Dreiding force field[12a] for aromatic π–π stacking energy $E_\pi$ and the first principles calculation at the B3LYP/6-311G(2d,p) level for all the other three energy components (Table 3). Our computations show that variations in varying energy components among all the structures are apparent with the largest variations of 28.6% and 11.5%

Table 3 Computationally determined energetic profiles[a] in kcal mol$^{-1}$ associated with the structures of **2**·2H$_2$O and **2**$_n$·2H$_2$O ($n$ = 1–4)

| Water complexes | $E_{SE}$ | $E_\pi$ | $E_{HG}$ | | | $E_H$ | | | $E_{Total}$ ($E_{SE}$ + $E_\pi$ + $E_{HG}$ + $E_H$) |
|---|---|---|---|---|---|---|---|---|---|
| | | | $E_{HG_a}$ | $E_{HG_b}$ | $E_{Total}$ | $E_{H_a}$ | $E_{H_b}$ | $E_{Total}$ | |
| **2**·2H$_2$O | 2.28 | 31.09 | 9.14 | 12.29 | 21.43 | 4.15 | 3.60 | 7.75 | 62.55 |
| **2**$_1$·2H$_2$O | 2.39 | 28.22 | 10.86 | 12.34 | 23.20 | 4.83 | 3.53 | 8.36 | 62.17 |
| **2**$_2$·2H$_2$O | 2.24 | 26.08 | 9.98 | 12.78 | 22.76 | 5.08 | 3.13 | 8.21 | 59.29 |
| **2**$_3$·2H$_2$O | 2.43 | 28.65 | 10.06 | 11.57 | 21.63 | 4.31 | 4.03 | 8.34 | 61.05 |
| **2**$_4$·2H$_2$O | 2.31 | 22.20 | 9.96 | 12.05 | 22.01 | 4.29 | 3.85 | 8.14 | 54.66 |
| Variation% | 7.8% | 28.6% | 15.8% | 9.5% | 11.5% | 18.3% | 22.3% | 7.3% | 12.6% |

[a] Every energy profile calculated include the H-bonds arising from the "sticky" ends ($E_{SE}$), aromatic π–π stacking interaction ($E_\pi$), stabilization of water molecules **a** and **b** (Fig. 3) by the hosts ($E_{HG}$), and the two types of H-bonds **H$_a$** and **H$_b$** (Fig. 3) contained in the water chains ($E_H$). The values for variation% were obtained by dividing the difference between the largest and smallest numbers using the largest number within the same category.

arising from aromatic π–π stacking ($E_\pi$) and host–guest ($E_{HG}$) interactions, respectively. Although the energetic variation in the total H-bond strength is much smaller (7.3%), which provides attractive forces to stabilize both the full overlap of helically folded aromatic backbones ($E_{SE}$) and the 1D water chains remaining ($E_H$), both of its two components $E_{H_a}$ and $E_{H_a}$ have very large variations of 18.3% and 22.3%, respectively. These data suggest that both the water chains and aquapores assembled from aquafoldamer molecules are very dynamic in structure and particularly in energy, and that the external stimuli such as the presence of excessive amounts of methanol during the crystal growth exert the largest impact on aromatic π–π stacking and a very substantial influence on both the intermolecular H-bonds in the 1D water chains and the host–guest interactions, while the H-bonds from the "sticky" ends remain much less affected. Further, it might be of additional interest to note that the water chain-containing aquapores, with their total energy, $E_{Total}$, ranging from 59.29 (**2**$_2$·2H$_2$O, Table 3) to 62.55 kcal mol$^{-1}$ (**2**·2H$_2$O, Table 3), seem to be robust enough to withstand methanol present in solution in a 19-fold excess in volume with respect to water, but a 39-fold excess of methanol likely produces a dramatic impact on the aquapore structure, leading to an abrupt decrease in its energy and stability with an $E_{Total}$ value of 54.66 kcal mol$^{-1}$.

Even more dramatic dynamics around the region involving "sticky ends" in the assembled aquapores can also be seen by comparing the crystal structure containing aligned methanol molecules **2**·MeOH with any other crystal structure containing 1D water chains such as **2**$_1$·2H$_2$O (Table 2 and Fig. 5). Each "sticky end" contains two types of H-bonds, **H$_1$** and **H$_2$**, and the two H-bonds from **2**·MeOH are either the shortest (2.405 Å) among the **H$_1$** types or the longest (3.018 Å) among the **H$_2$** types. More importantly, the **H$_1$** type H-bond is shorter than the **H$_2$** type H-bond in **2**·MeOH, and this relative magnitude is reversed in all the water-containing structures including **2**$_1$·2H$_2$O with the **H$_2$** type H-bond (2.799 Å, Fig. 5) being shorter than the **H$_1$** type (3.045 Å, Fig. 5). This suggests a significant re-arrangement of the "sticky end" in order for the same host **2** to accommodate water rather than methanol molecules in the assembled hollow cavity. By comparing the

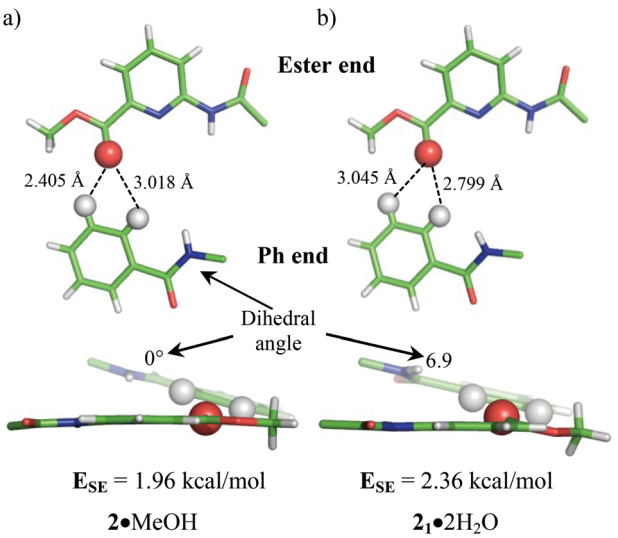


Fig. 5 Top and side views of the "sticky" ends in (a) **2**·MeOH and (b) **2**$_1$·2H$_2$O, which demonstrate significant differences around the "sticky" ends found in **2**·MeOH and **2**$_1$·2H$_2$O in order to accommodate MeOH and water molecules in their interiors. The "sticky" ends from other water-containing structures such as **2**·2H$_2$O, **2**$_2$·2H$_2$O, **2**$_3$·2H$_2$O and **2**$_4$·2H$_2$O have a near-identical look. Also see Fig. 4 for other differences in the helical backbone of **2** among **2**$_n$·2H$_2$O ($n$ = 1–4).

H-bond length of **H$_1$** and **H$_2$** types in **2**·MeOH respectively with those of **H$_2$** and **H$_1$** types in **2**$_1$·2H$_2$O (Fig. 5), the H-bonds in **2**·MeOH are apparently shorter overall. Surprisingly, the overall strength involving the two H-bonds in **2**·MeOH with a computationally determined value of 1.96 kcal mol$^{-1}$ is energetically less stable than that found in **2**$_1$·2H$_2$O by 0.40 kcal mol$^{-1}$ (Fig. 5). A careful comparison of the side views of the "sticky end" regions in **2**·MeOH and **2**$_1$·2H$_2$O reveals a very minor difference in planarity involving the three H-bond donor and acceptor atoms, *i.e.*, one carbonyl O-atom from the ester end and two aromatic H-atoms from the Ph end. In more detail, the carbonyl O-atom from the ester end of **2**·MeOH stays coplanar with the ester end, and therefore deviates from the aromatic plane of the Ph end that contains two H-atoms more

than the corresponding O-atom from $\mathbf{2_1}\cdot 2H_2O$ whose carbonyl O-atom slightly points away from the plane defined by the ester end and toward the two H-atoms. This seemingly more planar arrangement involving the three H-bond donor and acceptor atoms in $\mathbf{2_1}\cdot 2H_2O$ likely enhances the orbital overlapping extent among the donor and acceptor atoms, and increases the overall strength of the two H-bonds. A significant re-arrangement is additionally seen in the helically shaped aromatic backbone of **2** with parts of its helical backbone being comparatively more flat in **2**·MeOH than the corresponding parts in all the water-containing structures (Fig. 4).

## Experimental section

Pentamer **2** was synthesized using previously established procedures reported by us.[11c] All solvents were of reagent grade quality and used as supplied by the manufacturers.

### Crystallization experiments

X-ray quality crystals of **2**·MeOH were grown *via* slow diffusion of 0.9 mL MeOH into 0.6 mL dichloromethane containing 2 mg of **2** in a capped vial over 15 days at room temperature. And X-ray quality crystals of $\mathbf{2_n}\cdot 2H_2O$ ($n$ = 1–4) were grown *via* slow diffusion of a certain volume of MeOH/$H_2O$ at varying ratios into 1 mL of dichloromethane containing 1 mg of **2** in a capped vial over 10–15 days at room temperature.

### First principles computations

All the calculations except for the energy of aromatic π–π interactions were carried out on the structural motifs taken from the respective crystal structures by utilizing either the Gaussian 03[12b] or Gaussian 09[12c] program package. The Becke's three parameter hybrid functional with the Lee–Yang–Parr correlation functional (B3LYP)[12d] method was employed to carry out the calculations. Unless otherwise stated, the 6-311+G(2d, p)[12e] basic from the Gaussian basis set library has been used in all the single point energy calculations.

### Computations by the Dreiding force field[12a]

The Dreiding force field was used to calculate the energy of aromatic π–π interactions as tabulated in Table 3 with the corresponding structural motifs taken from the respective crystal structures. The convergence tolerance is $2 \times 10^{-5}$ kcal mol$^{-1}$ for the energy, 0.001 kcal mol$^{-1}$ A$^{-1}$ for the force, 0.001 GPa for the stress and $10^{-5}$ A for the displacement. The Ewald method is used for calculating the electrostatic and the van der Waals terms. The accuracy is $10^{-5}$ kcal mol$^{-1}$. The repulsive cutoff is 6 Å for the van der Waals term. For the hydrogen bond term, the summation method is atom based and the truncation method is a cubic spline with a cutoff distance of 4.5 Å.

### X-ray crystallography

X-ray single crystal data were collected on a Bruker APEX diffractometer with a CCD detector and graphite-monochromated MoKα radiation using a sealed tube (2.4 kW) at 223(2) K. Absorption corrections were made with the program SADABS[13a] and the crystallographic package SHELXTL[13b] was used for all calculations. CCDC numbers for **2**·MeOH, $\mathbf{2_1}\cdot 2H_2O$, $\mathbf{2_2}\cdot 2H_2O$, $\mathbf{2_3}\cdot 2H_2O$, and $\mathbf{2_4}\cdot 2H_2O$ are 1419114, 1419115, 1419116, 1419117 and 1419118, respectively.

## Conclusions

Although the hollow cavity in $(\mathbf{1})_n$ selectively recognizes guest molecules decreasing in the order of MeOH > $H_2O$ > $CH_2Cl_2$, a similar hollow cavity in $(\mathbf{2})_n$ created from the structurally similar molecules of **2** does not recognize $CH_2Cl_2$ at all, and displays a much higher affinity toward $H_2O$ than MeOH molecules. Contrary to the formation of a continuous H-bonded water chain in $(\mathbf{2}\cdot 2H_2O)_n$, methanol molecules are trapped inside the hollow cavity in $(\mathbf{2}\cdot\mathrm{MeOH})_n$ in a discrete fashion. By doping 10 to 800 μl of methanol into crystallization conditions containing 20 μl of water, both the structural dynamic and energy profile of water chain-containing aquapores formed from **2** under different conditions have been further studied. While the overall structures involving the water chains and aquapores remain stable and similar, these water chain-containing structures do undergo dynamic re-arrangements in response to varying amounts of methanol molecules and differ subtly in many aspects including the helical pitch, the average aromatic π–π stacking distance/strength, and the length/strength of the H-bonds responsible for inducing helical stacks and stabilizing 1D water chains. Energetically, the external stimuli seem to exert a substantial impact on the various structural motifs with the increasing order of the H-bonds from the "sticky" ends < the H-bonds in the 1D water chains or the host–guest interactions < the aromatic π–π stacking. Lastly, the one-dimensionally assembled aquapores dynamically undergo a significant re-arrangement in both the "sticky end" region and the helically shaped aromatic backbone in order to accommodate water, rather than methanol, molecules in their hollow cavities.

## Acknowledgements

Financial support by the Institute of Bioengineering and Nanotechnology (Biomedical Research Council, Agency for Science, Technology and Research, Singapore), the A*STAR Computational Resource Centre through the use of its high performance computing facilities and the National Natural Science Foundation of China (21172047 to Y. H.) is acknowledged.

## Notes and references

1 (*a*) K. Murata, K. Mitsuoka, T. Hirai, T. Walz, P. Agre, J. B. Heymann, A. Engel and Y. Fujiyoshi, *Nature*, 2000, **407**, 599; (*b*) E. Tajkhorshid, P. Nollert, M. Ø. Jensen,

 

L. J. W. Miercke, J. O'Connell, R. M. Stroud and K. Schulten, *Science*, 2002, **296**, 525.
2 M. Barboiu and A. Gilles, *Acc. Chem. Res.*, 2013, **46**, 2814.
3 (*a*) B. Henrik, S. Dieter and P. Philip, *Angew. Chem., Int. Ed.*, 2002, **41**, 754; (*b*) L. E. Cheruzel, M. S. Pometun, M. R. Cecil, M. S. Mashuta, R. J. Wittebort and R. M. Buchanan, *Angew. Chem., Int. Ed.*, 2003, **42**, 5452; (*c*) P. S. Sidhu, K. A. Udachin and J. A. Ripmeester, *Chem. Commun.*, 2004, 1358; (*d*) B. K. Saha and A. Nangia, *Chem. Commun.*, 2005, 3024; (*e*) K. Ono, K. Tsukamoto, R. Hosokawa, M. Kato, M. Suganuma, M. Tomura, K. Sako, K. Taga and K. Saito, *Nano Lett.*, 2009, **9**, 122; (*f*) Y. L. Duc, M. Michau, A. Gilles, V. Gence, Y.-M. Legrand, A. Lee, S. Tingry and M. Barboiu, *Angew. Chem., Int. Ed.*, 2011, **50**, 11366.
4 (*a*) U. S. Raghavender, S. Aravinda, N. Shamala, Kantharaju, R. Rai and P. Balaram, *J. Am. Chem. Soc.*, 2009, **131**, 15130; (*b*) U. S. Raghavender, Kantharaju, S. Aravinda, N. Shamala and P. Balaram, *J. Am. Chem. Soc.*, 2010, **132**, 1075; (*c*) R. Natarajan, J. P. H. Charmant, A. G. Orpen and A. P. Davis, *Angew. Chem., Int. Ed.*, 2010, **49**, 5125.
5 (*a*) M. S. Kaucher, M. Peterca, A. E. Dulcey, A. J. Kim, S. A. Vinogradov, D. A. Hammer, P. A. Heiney and V. Percec, *J. Am. Chem. Soc.*, 2007, **129**, 11698; (*b*) C. B. Hu, Z. X. Chen, G. F. Tang, J. L. Hou and Z. T. Li, *J. Am. Chem. Soc.*, 2012, **134**, 8384; (*c*) X. B. Zhou, G. D. Liu, K. Yamato, Y. Shen, R. X. Cheng, X. X. Wei, W. L. Bai, Y. Gao, H. Li, Y. Liu, F. T. Liu, D. M. Czajkowsky, J. F. Wang, M. J. Dabney, Z. H. Cai, J. Hu, F. V. Bright, L. He, X. C. Zeng, Z. F. Shao and B. Gong, *Nat. Commun.*, 2012, **3**, 949.
6 (*a*) A. J. Kim, M. S. Kaucher, K. P. Davis, M. Peterca, M. R. Imam, N. A. Christian, D. H. Levine, F. S. Bates, V. Percec and D. A. Hammer, *Adv. Funct. Mater.*, 2009, **19**, 2930; (*b*) W. Si, L. Chen, X. B. Hu, G. F. Tang, Z. X. Chen, J. L. Hou and Z. T. Li, *Angew. Chem., Int. Ed.*, 2011, **50**, 12564.
7 For some selected reviews in foldamers, see: (*a*) S. H. Gellman, *Acc. Chem. Res.*, 1998, **31**, 173; (*b*) D. J. Hill, M. J. Mio, R. B. Prince, T. S. Hughes and J. S. Moore, *Chem. Rev.*, 2001, **101**, 3893; (*c*) R. P. Cheng, S. H. Gellman and W. F. DeGrado, *Chem. Rev.*, 2001, **101**, 3219; (*d*) M. S. Cubberley and B. L. Iverson, *Curr. Opin. Chem. Biol.*, 2001, **5**, 650; (*e*) A. R. Sanford and B. Gong, *Curr. Org. Chem.*, 2003, **7**, 1649; (*f*) R. P. Cheng, *Curr. Opin. Struct. Biol.*, 2004, **14**, 512; (*g*) B. Gong, *Acc. Chem. Res.*, 2008, **41**, 1376; (*h*) Z. T. Li, J. L. Hou and C. Li, *Acc. Chem. Res.*, 2008, **41**, 1343; (*i*) W. S. Horne and S. H. Gellman, *Acc. Chem. Res.*, 2008, **41**, 1399; (*j*) I. Saraogi and A. D. Hamilton, *Chem. Soc. Rev.*, 2009, **38**, 1726; (*k*) G. Guichard and I. Huc, *Chem. Commun.*, 2011, **47**, 5933; (*l*) B. Baptiste, F. Godde and I. Huc, *ChemBioChem*, 2009, **10**, 1765; (*m*) K. Yamato, M. Kline and B. Gong, *Chem. Commun.*, 2012, **48**, 12142; (*n*) D.-W. Zhang, X. Zhao, J.-L. Hou and Z.-T. Li, *Chem. Rev.*, 2012, **112**, 5271; (*o*) W. Q. Ong and H. Q. Zeng, *J. Inclusion Phenom. Macrocyclic Chem.*, 2013, **76**, 1; (*p*) H. L. Fu, Y. Liu and H. Q. Zeng, *Chem. Commun.*, 2013, **49**, 4127.
8 For folding molecules derived from methoxybenzene, pyridone and fluorobenzene building blocks recently reported by us, see: (*a*) B. Qin, C. Sun, Y. Liu, J. Shen, R. J. Ye, J. Zhu, X.-F. Duan and H. Q. Zeng, *Org. Lett.*, 2011, **13**, 2270; (*b*) Y. Yan, B. Qin, Y. Y. Shu, X. Y. Chen, Y. K. Yip, D. W. Zhang, H. B. Su and H. Q. Zeng, *Org. Lett.*, 2009, **11**, 1201; (*c*) Y. Yan, B. Qin, C. L. Ren, X. Y. Chen, Y. K. Yip, R. J. Ye, D. W. Zhang, H. B. Su and H. Q. Zeng, *J. Am. Chem. Soc.*, 2010, **132**, 5869; (*d*) Z. Y. Du, C. L. Ren, R. J. Ye, J. Shen, Y. J. Lu, J. Wang and H. Q. Zeng, *Chem. Commun.*, 2011, **47**, 12488; (*e*) C. L. Ren, V. Maurizot, H. Q. Zhao, J. Shen, F. Zhou, W. Q. Ong, Z. Y. Du, K. Zhang, H. B. Su and H. Q. Zeng, *J. Am. Chem. Soc.*, 2011, **133**, 13930; (*f*) C. L. Ren, F. Zhou, B. Qin, R. J. Ye, S. Shen, H. B. Su and H. Q. Zeng, *Angew. Chem., Int. Ed.*, 2011, **50**, 10612; (*g*) C. L. Ren, S. Y. Xu, J. Xu, H. Y. Chen and H. Q. Zeng, *Org. Lett.*, 2011, **13**, 3840.
9 For various functions elaborated on the folding molecules over the recent years by us, see: (*a*) B. Qin, C. L. Ren, R. J. Ye, C. Sun, K. Chiad, X. Y. Chen, Z. Li, F. Xue, H. B. Su, G. A. Chass and H. Q. Zeng, *J. Am. Chem. Soc.*, 2010, **132**, 9564; (*b*) J. Shen, W. L. Ma, L. Yu, J.-B. Li, H.-C. Tao, K. Zhang and H. Q. Zeng, *Chem. Commun.*, 2014, **50**, 12730; (*c*) W. Q. Ong, H. Q. Zhao, C. Sun, J. E. Wu, Z. C. Wong, S. F. Y. Li, Y. H. Hong and H. Q. Zeng, *Chem. Commun.*, 2012, **48**, 6343; (*d*) C. Sun, C. L. Ren, Y. C. Wei, B. Qin and H. Q. Zeng, *Chem. Commun.*, 2013, **49**, 5307; (*e*) B. Qin, L. Y. Jiang, S. Shen, C. Sun, W. X. Yuan, S. F. Y. Li and H. Q. Zeng, *Org. Lett.*, 2011, **13**, 6212; (*f*) Z. Y. Du, B. Qin, C. Sun, Y. Liu, X. Zheng, K. Zhang, A. H. Conney and H. Q. Zeng, *Org. Biomol. Chem.*, 2012, **10**, 4164; (*g*) H. Q. Zhao, J. Shen, J. J. Guo, R. J. Ye and H. Q. Zeng, *Chem. Commun.*, 2013, **49**, 2323.
10 (*a*) W. Q. Ong, H. Q. Zhao, Z. Y. Du, J. Z. Y. Yeh, C. L. Ren, L. Z. W. Tan, K. Zhang and H. Q. Zeng, *Chem. Commun.*, 2011, **47**, 6416; (*b*) H. Q. Zhao, W. Q. Ong, X. Fang, F. Zhou, M. N. Hii, S. F. Y. Li, H. B. Su and H. Q. Zeng, *Org. Biomol. Chem.*, 2012, **10**, 1172; (*c*) W. Q. Ong, H. Q. Zhao, X. Fang, S. Woen, F. Zhou, W. L. Yap, H. B. Su, S. F. Y. Li and H. Q. Zeng, *Org. Lett.*, 2011, **13**, 3194.
11 (*a*) H. Q. Zhao, W. Q. Ong, F. Zhou, X. Fang, X. Y. Chen, S. F. Y. Li, H. B. Su, N.-J. Cho and H. Q. Zeng, *Chem. Sci.*, 2012, **3**, 2042; (*b*) F. Zhou, H. L. Fu, W. Q. Ong, R. J. Ye, W. X. Yuan, Y.-J. Lu, Y.-P. Huo, K. Zhang, H. B. Su and H. Q. Zeng, *Org. Biomol. Chem.*, 2012, **10**, 5525; (*c*) H. Q. Zhao, S. Sheng, Y. H. Hong and H. Q. Zeng, *J. Am. Chem. Soc.*, 2014, **136**, 14270.
12 (*a*) S. L. Mayo, B. D. Olafson and W. A. Goddard III, *J. Phys. Chem.*, 1990, **94**, 8897; (*b*) M. J. Frisch, in *Gaussian 03*, Gaussian, Inc., Wallingford, CT, 2004; (*c*) M. J. Frisch, in *Gaussian 09*, Gaussian, Inc., Wallingford, CT, 2009; (*d*) A. D. Becke, *J. Chem. Phys.*, 1993, **98**, 5648; (*e*) G. A. Petersson, A. Bennett, T. G. Tensfeldt, M. A. Al-Laham, W. A. Shirley and J. Mantzaris, *J. Chem. Phys.*, 1988, **89**, 2193.
13 (*a*) G. M. Sheldrick, *SADABS, Software for Empirical Absorption Corrections*, University of Göttingen, Germany, 2000; (*b*) *SHELXTL, Reference Manual, version 5.1*, Bruker AXS, Analytical X-Ray Systems, Madison, WI, USA, 1997.